

## Electrical activation and electron spin coherence of ultralow dose antimony implants in silicon

T. Schenkel,<sup>a)</sup> J. A. Liddle, and A. Persaud

*E. O. Lawrence Berkeley National Laboratory, Berkeley, California 94720*

A. M. Tyryshkin and S. A. Lyon

*Department of Electrical Engineering, Princeton University, Princeton, New Jersey 08544*

R. de Sousa and K. B. Whaley

*Department of Chemistry and Pitzer Center for Theoretical Chemistry, University of California, Berkeley, California 94720*

J. Bokor and J. Shangkuan

*E. O. Lawrence Berkeley National Laboratory, Berkeley, California 94720, and*

*Department of Electrical Engineering and Computer Science, University of California, Berkeley, California 94720*

I. Chakarov

*Silvaco International, 4701 Patrick Henry Drive, Santa Clara, California 95054*

(Received 14 July 2005; accepted 26 January 2006; published online 13 March 2006)

We implanted ultralow doses ( $2 \times 10^{11} \text{ cm}^{-2}$ ) of antimony ions ( $^{121}\text{Sb}$ ) into isotopically enriched silicon ( $^{28}\text{Si}$ ) and find high degrees of electrical activation and low levels of dopant diffusion after rapid thermal annealing. Pulsed electron spin resonance shows that spin echo decay is sensitive to the dopant depths, and the interface quality. At 5.2 K, a spin decoherence time,  $T_2$ , of 0.3 ms is found for profiles peaking 50 nm below a Si/SiO<sub>2</sub> interface, increasing to 0.75 ms when the surface is passivated with hydrogen. These measurements provide benchmark data for the development of devices in which quantum information is encoded in donor electron spins. © 2006 American Institute of Physics. [DOI: 10.1063/1.2182068]

Spins of electrons bound to donor atoms in silicon at low temperature are promising candidates for the development of quantum information processing devices.<sup>1–3</sup> This is due to their long decoherence times, and the potential to leverage fabrication finesse in a silicon transistor paradigm. Recently, relatively long transverse relaxation times ( $T_2$ ) were determined for electron spins in pulsed electron spin resonance (ESR) studies of phosphorous donors in isotopically enriched silicon. Here, donors were present as a random background doping across  $^{28}\text{Si}$  epilayers and  $T_2$  extrapolated to 60 ms for isolated donors.<sup>3</sup> Formation of test devices for quantum information processing requires the integration of individual dopant atoms with a control and readout infrastructure. Donor array fabrication is being addressed by ion implantation<sup>4–6</sup> and scanning probe based hydrogen lithography.<sup>7,8</sup> Dopant spacing depends on the choice of entangling interactions between quantum bits (qubits) and ranges from 20 to over 100 nm, corresponding to ultralow ion implantation doses of  $<10^{10}$  to  $2.5 \times 10^{11} \text{ cm}^{-2}$ . In this letter, we report on depth profiles and electrical activation following rapid thermal annealing (RTA) of ultralow dose  $^{121}\text{Sb}$  implants and correlate electron spin relaxation times with the dopant distribution below an interface and with the interface quality.

We processed wafers with 10  $\mu\text{m}$  thick,  $^{28}\text{Si}$  enriched epilayers (500 ppm  $^{29}\text{Si}$ ) on *p*-type natural silicon (100) and natural silicon control wafers (100), both with impurity concentrations  $\leq 10^{14} \text{ cm}^{-3}$ . Standard processes were followed for formation of 5–10 nm thick thermal SiO<sub>2</sub>. Typical den-

sities of trapped charges and interface traps were  $1\text{--}2 \times 10^{11} \text{ cm}^{-2}$  for the thermal oxides.  $^{121}\text{Sb}$  ion implantation with a dose of  $2 \times 10^{11} \text{ cm}^{-2}$  was conducted with implant energies of 120 and 400 keV.  $^{121}\text{Sb}$  was used to avoid any ambiguity of results due to  $^{31}\text{P}$  background in  $^{28}\text{Si}$  epilayers. RTA for repair of implant damage and substitutional incorporation of dopants into the silicon lattice, i.e., electrical activation, was performed with an AGA Heatpulse 610. Following annealing, carrier depth profiles were probed with spreading resistance analysis (SRA).<sup>9</sup> Secondary ion mass spectrometry (SIMS)<sup>9</sup> was used to characterize elemental depth profiles in as-implanted and annealed samples. As-implanted depth profiles were also simulated using a dynamic Monte Carlo model.<sup>10</sup> Electron spin relaxation in  $^{28}\text{Si}$  samples was probed by pulsed ESR in an *X*-band (9.7 GHz) Bruker EPR spectrometer at temperatures of 5–10 K. Standard inversion recovery and two-pulse echo experiments were used to measure  $T_1$  and  $T_2$  relaxation times, respectively.<sup>3</sup>

Figure 1(a) shows SIMS and SRA depth profiles of a  $^{28}\text{Si}$  sample implanted with  $^{121}\text{Sb}$  at 400 keV (0° tilt) and a dose of  $2 \times 10^{11} \text{ cm}^{-2}$ , together with a simulation of the as-implanted profile. The sample was annealed in an N<sub>2</sub>/H<sub>2</sub> ambient at 980 °C for 7 s. We define the electrical activation ratio as the ratio between the carriers from an integrated, background corrected SRA profile, and the implanted dose. Nominal implant doses agreed with values extracted from SIMS spectra. The electrical activation of donors in the  $^{28}\text{Si}$  sample is complete, i.e., 100%, within the accuracy of the measurements.

<sup>a)</sup>Electronic mail: t\_schenkel@lbl.gov

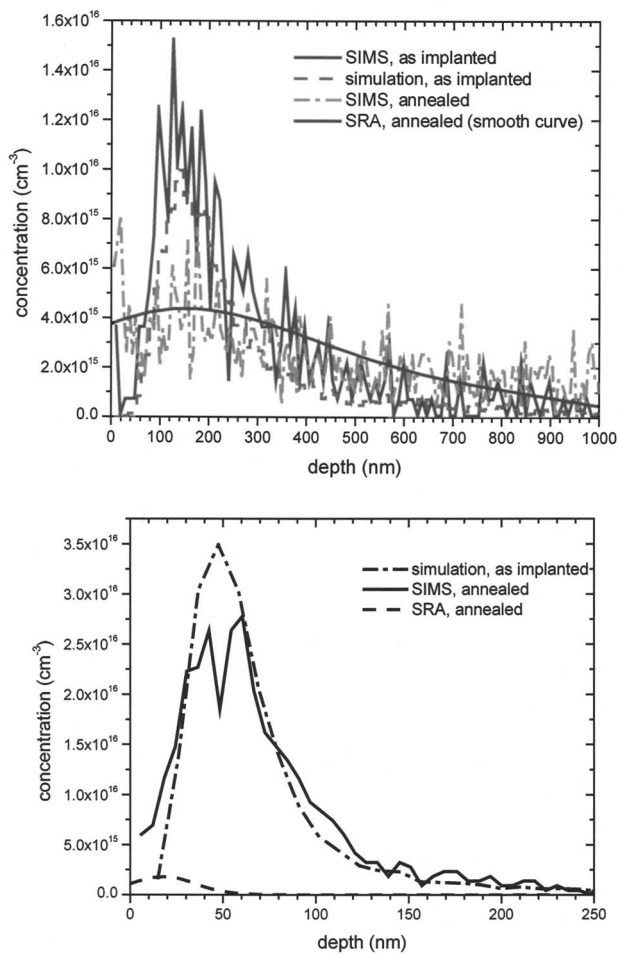


FIG. 1. (a) SIMS and SRA profiles of as-implanted and annealed samples together with simulated depth profiles for antimony ( $^{121}\text{Sb}$ ) implanted to a dose of  $2 \times 10^{11} \text{ cm}^{-2}$  with an implant energy of: (a) 400 keV  $^{121}\text{Sb}$  and (b) 120 keV.

Due to low donor concentrations of  $10^{16} \text{ cm}^{-3}$  and below, the SIMS spectra are relatively noisy and yet allow some definite conclusions. The as-implanted SIMS spectrum matches the simulated depth profile closely, but the SIMS spectrum of the annealed  $^{28}\text{Si}$  sample shows significant broadening compared to the as-implanted profile. This broadening is reproduced in the SRA profile. We attribute the profile broadening to diffusion during annealing. The profile broadening is symmetrical and there is no evidence for segregation of dopants toward the Si/SiO<sub>2</sub> interface. This is important for dopant array retention in future qubit devices and in stark contrast to observations of pronounced phosphorus segregation toward Si/SiO<sub>2</sub> interfaces during annealing.<sup>5</sup> Antimony diffuses through a vacancy mechanism and diffusion is retarded by the interstitials injected from the Si/SiO<sub>2</sub> interface during annealing.<sup>11,12</sup>

In Fig. 1(b), we show SIMS, SRA, and simulated depth profiles from samples implanted with  $^{121}\text{Sb}$  ( $2 \times 10^{11} \text{ cm}^{-2}$ ) at 120 keV ( $7^\circ$  tilt). The sample was annealed in a N<sub>2</sub> ambient at 1000 °C for 10 s. Simulations of the as-implanted profile and the SIMS profile of the annealed sample agree very well. SIMS spectra of the as-implanted samples were not available. The close agreement between the simulated as-implanted, and the SIMS profile of the annealed sample indicates only minimal diffusion and no segregation of donors to the interface.

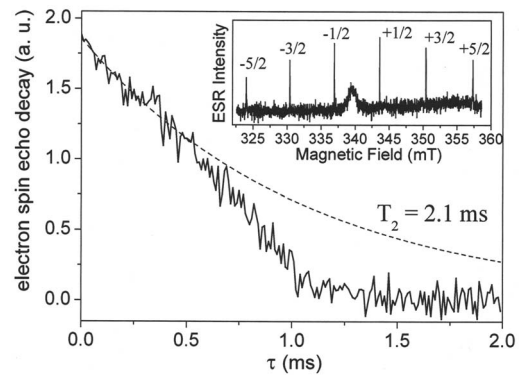


FIG. 2. The two-pulse electron spin echo (ESE) decay for  $^{121}\text{Sb}$  donors in  $^{28}\text{Si}$  (400 keV, dose  $2 \times 10^{11} \text{ cm}^{-2}$ , annealed) measured at the  $M = +\frac{1}{2}$  line in the ESR spectrum at 5.2 K. Because the ESE signal decay is strongly suppressed at long  $\tau > 0.5$  ms by magnetic field noise (Ref. 3), the exponential fit (dashed line) was calculated using only  $\tau < 0.5$  ms and resulted in  $T_2 = 2.1$  ms. The inset shows an ESR spectrum of  $^{121}\text{Sb}$ , consisting of six narrow ( $< 0.2$  G) lines split by hyperfine interaction with the nuclear spin ( $I = 5/2$ ) of  $^{121}\text{Sb}$ . The broad feature in the center of the spectrum is from surface defects due to sample preparation.

In contrast to the SIMS data, the SRA spectrum shows a carrier distribution that is strongly shifted toward the surface, and the apparent electrical activation is only 3%. However, repeated SRA measurements on these samples showed inconsistent results. The apparent low carrier concentrations in SRA were consistent with spin counts in ESR measurements. Signal in both SRA and ESR stems from donors that are incorporated on substitutional sites in the silicon lattice and that are electrically neutral. Band bending at the interface due to interface and oxide charges leads to the ionization of donors close to the interface and thus to the reduced number of active donors seen by both SRA and ESR. Evidence for donor ionization are ESR experiments where sample illumination increased the spin counts significantly for the same samples with apparent low electrical activation levels in SRA. Based on this sample illumination effect on the spin count in ESR and the absence of dopant segregation to the interface in the SIMS results we estimate that the actual electrical activation of the 120 keV implants was also close to 100%.

Electron spin relaxation times were measured for shallower (120 keV implant energy, peak dopant depth of 50 nm) and deeper (400 keV implant energy, peak dopant depth of 150 nm)  $^{121}\text{Sb}$  implants in  $^{28}\text{Si}$  samples with thermal SiO<sub>2</sub> interfaces. The inset of Fig. 2 shows the six-line ESR spectrum of implanted  $^{121}\text{Sb}$  donors with splitting arising from hyperfine interaction with the nuclear spin ( $I = 5/2$ ) of  $^{121}\text{Sb}$ . Most of the relaxation measurements were done at the  $M = \frac{1}{2}$  hyperfine line but the relaxation times were identical on other lines. For shallower donors, we found spin relaxation times  $T_1 = 15 \pm 2$  ms and  $T_2 = 0.3 \pm 0.03$  ms at 5.2 K. For deeper implants, a much longer  $T_2 = 1.5 \pm 0.1$  ms was measured while the spin-lattice relaxation time,  $T_1 = 16 \pm 1$  ms, did not change.

The thermal oxide layer of  $^{28}\text{Si}$  samples was then removed by etching in a hydrofluoric acid solution, resulting in a hydrogen terminated silicon (100) surface of modest quality (compared to Si-111).<sup>13,14</sup> The electrical properties of the H-Si interface were not probed here, but typical surface charge densities below  $10^9 \text{ cm}^{-2}$  have previously been

TABLE I. Summary of apparent activation ratios from SRA and decoherence times for oxide and hydrogen passivation of  $^{28}\text{Si}$  surfaces (100). Increased spin counts in ESR measurements under illumination indicate that the actual activation ratio is close to 100% also for the 120 keV implants.

Interface	Peak dopant depth (nm)	Apparent activation ratio	$T_1$ (ms) at 5.2 K	$T_2$ (ms) at 5.2 K
$\text{SiO}_2$	50	(3.4%)	$15 \pm 2$	$0.3 \pm 0.03$
H-Si	50	—	$16 \pm 2$	$0.75 \pm 0.04$
$\text{SiO}_2$	150	100%	$16 \pm 1$	$1.5 \pm 0.1$
H-Si	150	—	$14 \pm 1$	$2.1 \pm 0.1$

reported.<sup>15</sup> Following hydrogen passivation,  $T_2$  increased to 2.1 ms for the 400 keV implants, and to 0.75 ms for the 120 keV implants. We summarize our results in Table I.

Dopants diffuse through interaction with interstitials and vacancies. In the ultralow dose implant regime, dopant redistribution during rapid thermal annealing is affected by defect injection from the dielectric-silicon interface, and by the interaction of dopants with point defects that did not recombine following the slowdown of implanted ions (i.e., transient enhanced diffusion).<sup>11,12,16</sup> For the heavier antimony ions, point defect formation is enhanced in collision cascades compared to implantation of boron or phosphorus. Recombination of vacancies and interstitials is incomplete for ultralow dose implants.<sup>16</sup> From SIMS measurements and simulations we find that dopant redistribution is minimal for the 120 keV implants. The enhanced diffusion for the 400 keV implants might be a result of less complete recombination of vacancies and interstitials in more extended collision cascades formed by higher energy ions.

Quantum computer test structures require both efficient electrical activation of dopants and retention of initial dopant positions during thermal processing. The results shown here fulfill these requirements, and enable testing of single spin readout architectures with high device yields. Probing of spin dynamics in shallow donor implants requires gate control over energy levels to avoid donor ionization due to band bending, e.g., by tuning into a flatband condition.

Donor electron spin relaxation is correlated both with the depth distribution of dopants with respect to an interface and with the interface quality (Table I). The fact that removal of the oxide layer and H passivation of the interface lead to a significant increase in  $T_2$  allows us to conclude that it is coupling to paramagnetic defects<sup>17</sup> in the oxide and at the Si/SiO<sub>2</sub> interface which limits  $T_2$  for both shallow and deeper dopant distributions. A likely mechanism is fluctuating magnetic fields due to spin flips of paramagnetic defects and the loading and unloading of traps at the interface and in the oxide. At much reduced interface trap levels for the H-Si surface, coherence is likely limited by instantaneous diffusion, i.e., magnetic dipole coupling of neighboring dopant atoms,<sup>2,3</sup> and possibly other effects that have not been quantified. The effect of nuclear spins of hydrogen atoms at a coverage of  $6.8 \times 10^{14} \text{ cm}^{-2}$  for an H-Si(100) surface on donor electron spin coherence can be estimated with a spectral diffusion model.<sup>2</sup> This process is expected to limit  $T_2$

only for times longer than 1 s for the profiles shown in Fig. 1 and is probably not important in the present case, but will become important for shallower implants.

In summary, annealing of ultralow dose antimony implants in isotopically enriched  $^{28}\text{Si}$  leads to high degrees of electrical activation with minimal diffusion. The transverse electron spin relaxation time,  $T_2$ , increases when dopants are placed deeper below a thermal SiO<sub>2</sub> interface, and hydrogen passivation of the silicon surface yields an even longer  $T_2$  of 2.1 ms (at 5.2 K), indicating that spin flips in paramagnetic defects limit coherence in the presence of a Si/SiO<sub>2</sub> interface. Spin coherence times well in excess of 1 ms are readily achieved with standard silicon processing, enabling tests of quantum information processing architectures with donor electron spin qubits.

The authors thank T. C. Shen for many stimulating discussions, and the staff of the UC Berkeley Microlab for their technical support. This work was supported by NSA under ARO Contract No. MOD707501, the Department of Energy under Contract No. DE-AC02-05CH11231, and by NSF under Grant No. 0404208. Work at Princeton was supported by ARO and ARDA under Contract No. DAAD19-02-1-0040. K.B.W. and R.dS. acknowledge support by the DARPA SPINs program under Grant No. FDN0014-01-1-0826.

<sup>1</sup>B. E. Kane, *Nature (London)* **393**, 133 (1998); R. Vrijen, E. Yablonovitch, K. Wang, H. W. Jiang, A. Balandin, V. Roychowdhury, T. Mor, and D. DiVincenzo, *Phys. Rev. A* **62**, 012306 (2000).

<sup>2</sup>S. Das Sarma, R. de Sousa, X. Hu, and B. Koiller, *Solid State Commun.* **133**, 737 (2005).

<sup>3</sup>A. M. Tyryshkin, S. A. Lyon, A. V. Astashkin, and A. M. Raitsimring, *Phys. Rev. B* **68**, 193207 (2003).

<sup>4</sup>A. Persaud, S. J. Park, J. A. Liddle, J. Bokor, I. W. Rangelow, and T. Schenkel, *Nano Lett.* **5**, 1087 (2005).

<sup>5</sup>A. Persaud, S. J. Park, J. A. Liddle, I. W. Rangelow, J. Bokor, R. Keller, F. I. Allen, D. H. Schneider, and T. Schenkel, *Quantum Inf. Process.* **3**, 233 (2004); S.-J. Park, A. Persaud, J. A. Liddle, J. Nilsson, J. Bokor, D. H. Schneider, I. Rangelow, and T. Schenkel, *Microelectron. Eng.* **73-74**, 695 (2004).

<sup>6</sup>D. N. Jamieson, C. Yang, T. Hopf, S. M. Hearne, C. I. Pakes, S. Prawer, M. Mitic, E. Gauja, S. E. Andersen, F. E. Hudson, A. S. Dzurak, and R. G. Clark, *Appl. Phys. Lett.* **86**, 202101 (2005).

<sup>7</sup>T. C. Shen, J. S. Kline, T. Schenkel, S. J. Robinson, J.-Y. Ji, C. Yang, R.-R. Du, and J. R. Tucker, *J. Vac. Sci. Technol. B* **22**, 3182 (2004).

<sup>8</sup>F. J. Ruess, L. Overbeck, M. Y. Simmons, K. E. J. Goh, A. R. Hamilton, T. Hallam, S. R. Schofield, N. J. Curson, and R. G. Clark, *Nano Lett.* **4**, 1969 (2004).

<sup>9</sup>Cascade Scientific, Ltd.

<sup>10</sup>I. R. Chakarov and R. P. Webb, *Radiat. Eff. Defects Solids* **130**, 447 (1994).

<sup>11</sup>N. Cowern and C. Rafferty, *MRS Bull.* **25**, 39 (2000).

<sup>12</sup>A. Ural, P. B. Griffin, and J. D. Plummer, *J. Appl. Phys.* **85**, 6440 (1999).

<sup>13</sup>J. C. Kim, J.-Y. Ji, J. S. Kline, J. R. Tucker, and T.-C. Shen, *Appl. Surf. Sci.* **220**, 293 (2003).

<sup>14</sup>K. Eng, R. N. McFarland, and B. E. Kane, *Appl. Phys. Lett.* **87**, 052106 (2005).

<sup>15</sup>E. Yablonovitch, D. L. Allara, C. C. Chang, T. Gmitter, and T. B. Bright, *Phys. Rev. Lett.* **57**, 249 (1986).

<sup>16</sup>L. Pelaz, G. H. Gilmer, V. C. Venezia, H. J. Gossman, M. Jaraiz, and J. Barbolla, *Appl. Phys. Lett.* **74**, 2017 (1999).

<sup>17</sup>S. T. Chang, J. K. Wu, and S. A. Lyon, *Appl. Phys. Lett.* **48**, 662 (1986); A. Stesmans and V. V. Afanas'ev, *Phys. Rev. B* **57**, 10030 (1998).